PHYSICAL REVIEW B VOLUME 17, NUMBER 4 15 FEBRUARY 1978

Resonant Raman scattering in GaAs

R. Trommer and M. Cardona
Max-Planck-Institut für Festkörperforschung, 7000 Stuttgart 80, Germany
(Received 19 September 1977)

We report measurements of resonant first- and second-order Raman scattering in GaAs with exciting photon energies covering the entire visible spectrum. Two sets of energy gaps were investigated: the three-dimensional $E_0/E_0+\Delta_0$ and the two-dimensional $E_1/E_1+\Delta_1$ critical points. The symmetry components of the second-order spectrum were separated and observed structures were interpreted by comparison with neutron scattering data. For a theoretical description of the Raman cross section we used either experimental values or a model description of the electric susceptibility. The resonance behavior could be explained for nearly all observed scattering processes with the exception of 2LO(Γ) and forbidden LO scattering by assuming for first order the electron–one-phonon and for second order the renormalized electron–two-phonon deformation potential coupling. Second-order deformation potentials are given as well as a comparison of the theoretically and experimentally determined ratios of the electron–one-phonon deformation potential near L to that near Γ. Forbidden LO scattering is explained well by the Fröhlich coupling mechanism, not only its resonance shape near $E_0+\Delta_0$ and near E_1 but also the ratio of its strength to that of TO scattering. 2LO (Γ) scattering is attributed to an iterated electron–one-phonon scattering process caused also by the Fröhlich interaction.

I. INTRODUCTION

Resonant Raman scattering has proven during the last years to be a useful tool in studying the electron-phonon interaction in diamond and zinc-blende structure semiconductors. For this family of materials the behavior of the Raman cross section has been investigated mainly near two sets of energy gaps in the electronic band structure: the three-dimensional $E_0/E_0+\Delta_0$ critical points at the Γ point of the Brillouin zone and the two-dimensional $E_1/E_1+\Delta_1$ critical points along its Λ direction, depending on which one of these sets of critical points occurs within the range of available tunable lasers. First-order Raman scattering by TO and LO(Γ) phonons in Ge,[1] Si,[2] GaP,[3] and the zinc chalcogenides[4,5] showed that the electron–one-phonon interaction is mainly due to deformation potential coupling, that means to the modulation of the electronic energy states caused by the periodic lattice deformation of a phonon. Intra- and interband scattering is possible; these mechanisms are equivalent to a pure energy modulation or to a mixing of electronic states by the phonon, respectively. The dielectric theory of Raman scattering shows the two-band term in the Raman tensor to be proportional to the first derivative of the electric susceptibiltiy χ with respect to the gap energy. The usual type of three-band term, due to coupling across a spin-orbit-split gap, is proportional to the difference $\chi^+-\chi^-$, where χ^+ and χ^- are the contributions of the spin-orbit-split $E_0/E_0+\Delta_0$ or $E_1/E_1+\Delta_1$ band transitions to χ. Hence the resonance line shapes can be calculated if the spectral dependence of the real and imaginary parts of χ are known. Due to the weak structure in the susceptibility near the E_0 gaps it is more practicable to use in this photon energy region instead of experimental data a model description for χ. In the zinc chalcogenides and other II-VI compounds this description has to take into account an exciton contribution. With increasing ionicity of the crystal the Fröhlich interaction of an electron with the macroscopic electric field of a LO phonon contributes more strongly to the electron–LO-phonon coupling. Its interband term, related to the first-order electro-optical effect, gives rise to a stronger LO than TO scattering cross section in allowed scattering configuration.[6] Bell[7] showed that its dispersion below the E_0 gap is nearly the same as that for the deformation potential term. In contrast, the interband Fröhlich coupling is a "forbidden effect" (its efficiency is proportional to the square of the momentum transfer) and gives rise to a much sharper resonance behavior of the LO phonon scattering observed in forbidden configuration. The Raman tensor for this mechanism is proportional to $d^2\chi/d\omega^2$. Recently, Gogolin and Rashba[8] proposed, however, that the observed forbidden LO scattering is rather due to an interaction of the electron with an impurity or an accoustic phonon before it is scattered by the LO phonon.

The second-order Raman spectrum is composed for diamond or zinc-blende structure materials of three symmetric components: Γ_1, Γ_{12} and $\Gamma_{25'}$ (for diamond), or Γ_{15} (for zinc-blende). While the Γ_{12} component was found in all investigated crystals[9-12] to be negligible, the dominating Γ_1 spectrum is mainly due to scattering by overtones

of phonons with high density of states [with the exception of a 2LO(Γ) peak]. In the $\Gamma_{25'}$ (Γ_{15}) spectrum mostly scattering by phonon combinations was found. The corresponding cross sections showed a resonance behavior similar to that of the first-order peak. Thus, the electron–two-phonon coupling mechanism was found to be of the deformation potential type with the electron–two-phonon interaction in first order. Several electron–two-phonon deformation potentials could be evaluated from the ratio of second- to first-order scattering intensities. The mentioned 2LO (Γ) peak was interpreted as due to an iterative electron–one-phonon scattering process via the Fröhlich coupling.

In this paper we present resonant Raman experiments in GaAs with exciting photon energies covering the range from 1.44 to 3.05 eV. The advantage of studying GaAs is, besides its model character as a III-V compound and its technological importance, the fact that, in contrast to the other so far investigated substances, both sets of gaps ($E_0/E_0+\Delta_0$ and $E_1/E_1+\Delta_1$) could be reached by cw ion and partly also by dye lasers. Thus it is possible to compare a great number of different electron-phonon interactions at different electronic gaps not only qualitatively but also quantitatively. We studied the resonance of allowed first-order scattering near E_0, $E_0+\Delta_0$, E_1, and $E_1+\Delta_1$ and that of forbidden LO scattering near $E_0+\Delta_0$ and near E_1. The resonance behavior of the second-order spectrum could be completely observed near E_1; near $E_0+\Delta_0$ only that of 2TO and 2LO (Γ) scattering. The relative change in the 2TO spectrum, which can be attributed to resonances at the indirect $\Gamma_8^v \rightarrow X_6^c$ and $\Gamma_8^v \rightarrow L_6^c$ transitions, has been reported elsewhere.[13]

We give a comparison of the experimentally obtained ratio of the electron–one-phonon deformation potential near Γ to that near L with theoretical evaluations. Our experimentally obtained ratio of 1TO to forbidden LO scattering intensities near $E_0+\Delta_0$ and near E_1 is in good agreement with theoretical predictions if one assumes only intraband LO scattering via the Fröhlich coupling mechanism. Finally a number of electron–two-phonon deformation potentials was evaluated.

II. THEORY

A. Deformation-potential mechanism

The theory of resonant first- and second-order Raman scattering near the E_0 and E_1 critical points has been treated by several authors.[3,4,10,14-17] The equivalence of describing the deformation-potential mechanism for first-order scattering by either time dependent third-order perturbation theory or by the dielectric theory has been proven within the quasistatic approximation.[18] First-order scattering is allowed in Γ_{15} symmetry. The expressions for second-order scattering are derived by assuming a renormalized electron–two-phonon interaction, that means both scattering phonons are created or destroyed within one process which may, nevertheless, have a dressed or composite vertex. The modulation or mixing of the electronic states is then given as a function of the phonon amplitudes and only one electron–two-phonon deformation potential. Our measured first- and second-order scattering intensities per incoming light power are given by[14]

$$I_1 = A[(1-R)^2/n^2]L(n_{B1}+1)\omega^4 |\vec{e}_s \vec{R}_1 \vec{e}_i|^2 , \tag{1}$$

$$I_2 = A[(1-R)^2/n^2]L(n_{B21}+1) \times (n_{B22}+1)\omega^4 \tfrac{1}{2} N\eta |\vec{e}_s \vec{R}_2 \vec{e}_i|^2 . \tag{2}$$

A is a constant which contains the experimental geometry factor plus physical constants, R is the reflection coefficient, n the refractive index, L the effective penetration depth of the light inside the crystal as given by Loudon, n_B is the Bose population factor, ω the photon frequency, N the number of unit cells, η the degeneracy of the scattering phonon branch, $\vec{e}_i$ and $\vec{e}_s$ the unit vectors in polarization direction of incoming and scattered light and $\vec{R}$ the Raman tensor (for the second-order scattering we use a Raman tensor *averaged* over all modes involved). We denote the Raman tensor components for first- and second-order scattering in Γ_1, Γ_{12}, and Γ_{15} symmetry as a_2, b_2 and d_1, d_2 with the index 1 standing for first and 2 standing for second order. The results are given as a function of the electric susceptibility χ.

1. $E_0/E_0+\Delta_0$

$$d_1 = \sqrt{3}\left(-\frac{d\chi^+}{d\omega_0} + 2\frac{\chi^+ - \chi^-}{\Delta_0}\right) d_0 \frac{u_0}{a_0} , \tag{3}$$

$$a_2 = \tfrac{4}{3}\, d\chi/d\omega_0 D_1 u_{01} u_{02}/{a_0}^2 , \tag{4}$$

$$b_2 = 6\sqrt{3}\left(-\frac{d\chi^+}{d\omega_0} + 2\frac{\chi^+ - \chi^-}{\Delta_0}\right) D_{12} \frac{u_{01}u_{02}}{a_0^2} , \tag{5}$$

$$d_2 = 2\sqrt{3}\left(-\frac{d\chi^+}{d\omega_0} + 2\frac{\chi^+ - \chi^-}{\Delta_0}\right) D_{15} \frac{u_{01}u_{02}}{a_0^2} . \tag{6}$$

Here $2\chi^+$ is the contribution of the E_0, χ^- that of the $E_0+\Delta_0$ critical point to the susceptibility, a_0 is the cubic lattice constant. The deformation potentials d_0, D_1, D_{12}, and D_{15} are defined in Refs. 3 and 18. u_0' is the zero-point vibrational amplitude of a phonon of energy Ω which is given by the expression[19]

$$u_0 = (4MN\Omega)^{-1/2} . \quad (7)$$

In the case of equal masses of the atoms sitting on the two different sublattices of a zinc-blende structure crystal M is simply two times their reduced mass for all vibrations. This also can be assumed to hold for GaAs since the masses of both constituent elements are very close. Two- and three-band processes across spin-orbit-split gaps are allowed in Γ_{12} and Γ_{15} symmetry, whereas in Γ_1 symmetry only intraband scattering is significant. For both intra- and interband scattering there exists only one independent deformation potential near E_0. Because the separation of experimental χ values into χ^+ and χ^- is difficult near $E_0/E_0+\Delta_0$, a model description can be used. The susceptibility χ due to a single degenerate three-dimensional critical point at frequency ω_0 is given by Cardona as[15]

$$\chi = \frac{1}{4\pi}\frac{P^2}{3}\left(\frac{2m^*}{\omega_0}\right)^{3/2}\left(\frac{\omega_0}{\omega}\right)^2 \times\left[2-\left(1+\frac{\omega}{\omega_0}\right)^{1/2}-\left(1-\frac{\omega}{\omega_0}\right)^{1/2}\right]. \quad (8)$$

where P is the matrix element for the transitions and m^* the reduced mass of the electron and the hole.

In a polar crystal an additional exciton contribution has to be considered. It is given for the $1s$ state of a Wannier exciton as[4]

$$\chi_{ex} = 8P^2/3\pi\,(m^*/\epsilon_\infty{}^3)\,[\omega_{ex}(\omega_{ex}^2-\omega^2)]^{-1} . \quad (9)$$

E_∞ is the high frequency dielectric constant and $\omega_{ex} = \omega_0 -$ (binding energy of the exciton).

In Γ_{15} symmetry the electron-phonon coupling takes place only within or between the valence bands. The centroid of these bands is not affected by this coupling and thus the electron mass is not modulated by the phonon. Since m^* is mainly due to the electron mass m^* stays also approximately unmodulated. However, in Γ_1 symmetry the energy of the gap itself is modulated by the phonon and with it the mass. Therefore, in this case the ratio m^*/ω_0 is to be taken as constant in deriving $d\chi/d\omega_0$.

2. $E_1/E_1+\Delta_1$

In the vicinity of the $E_1/E_1+\Delta_1$ critical points the Raman tensor components are given by the following expressions[10]:

$$d_1 = \left(\frac{2\sqrt{2}}{\sqrt{3}}\frac{\chi^+-\chi^-}{\Delta_1}d^5_{3,0}-\frac{1}{2\sqrt{3}}\frac{d\chi}{d\omega_1}d^5_{1,0}\right)\frac{u_0}{a_0} , \quad (10)$$

$$a_2 = \frac{4}{3}\frac{d\chi}{d\omega_1}D_1\frac{u_{01}u_{02}}{a_0{}^2} , \quad (11)$$

$$b_2 = \frac{8}{3}\frac{\chi^+-\chi^-}{\Delta_1}D_3^3\frac{u_{01}u_{02}}{a_0{}^2} , \quad (12)$$

$$d_2 = \frac{8}{\sqrt{3}}\left(\frac{\chi^+-\chi^-}{\Delta_1}D_3^5-\frac{1}{4\sqrt{2}}\frac{d\chi}{d\omega_1}D_1^5\right)\frac{u_{01}u_{02}}{a_0{}^2} . \quad (13)$$

The two two- and three-band deformation potentials which appear in these equations are, contrary to the E_0 gaps discussed above, independent of each other. For the deformation potentials d and D we have used the notation of Kane.[20]

B. Forbidden intraband scattering by LO phonons

1. $E_0/E_0+\Delta_0$

We consider here only the contribution of the Fröhlich coupling mechanism to forbidden intraband scattering by LO phonons. The Raman tensor is of fourth rank. Its resonance behavior near a three-dimensional critical point has been theoretically treated earlier.[16] For isotropic bands near the Γ point, the Raman tensor is diagonal so that a contribution of this coupling mechanism to Raman scattering is observed only for parallel-parallel polarized incident and scattered light. This is the case for the conduction and the lower of the spin-orbit-split valence bands in GaAs, not for transitions involving the upper degenerate Γ_8 valence bands. Thus the nondegenerate (except for spin) $E_0+\Delta_0$ gap is well suited as a model transition for investigations of Fröhlich interaction induced forbidden scattering. Within the framework of third-order perturbation theory, Zeyher arrives to a result for the diagonal component of the Raman tensor which can be written as follows[16]:

$$\vec{R}_F = \frac{qC_F}{12\pi\omega^2}\frac{P^2}{3}(S_e-S_h)(\Omega_{LO})^{-3/2}(2m^*)^{1/2} \times\left[\left(\frac{\omega_0-\omega-i\eta}{\Omega_{LO}}\right)^{1/2}-\left(\frac{\omega_0-\omega+\Omega_{LO}-i\eta}{\Omega_{LO}}\right)^{1/2}\right]^3 , \quad (14)$$

where q is the wave vector of the phonon, C_F the Fröhlich coupling constant (see Ref. 17), $s_e = m_e/(m_e+m_h)$, $s_h = m_h/(m_e+m_h)$ with m_e and m_h the electron and hole effective masses, Ω_{LO} the phonon frequency and η an energy broadening. If one compares the expression in parentheses with the most dispersive term in Eq. (8) one can easily see that it is proportional to the first derivative of the electric susceptibility with respect to the photon energy. Moreover, its third power is proportional to the second derivative of χ. Thus the diagonal Raman tensor component can finally be given near a three-dimensional critical point as

$$\vec{R}_F = \tfrac{1}{12}(qC_F/m^*)(S_e-S_h)(d^2\chi/d\omega^2) . \quad (15)$$

2. $E_1/E_1+\Delta_1$

In the case of a two-dimensional critical point like the E_1 or $E_1+\Delta_1$ band gap in GaAs, the transition probability given by perturbation theory (see Ref. 16) has to be integrated only over k directions perpendicular to the four equivalent $\langle 111\rangle$ directions of the Brillouin zone. Integration along the Λ directions can be considered as a multiplication with $\frac{3}{4}$ of the Brillouin-zone diameter, the active part of the E_1 transition along which the valence and conduction bands are parallel. If we now sum over the four valleys the Raman tensor near a two-dimensional critical point of energy ω_1 is given by

$$\vec{\vec{R}}_F = -\frac{\sqrt{3}}{4\pi}\frac{C_F}{q}(S_e - S_h)\Omega_{LO}^{-2}\frac{1}{a_0}\left(\frac{\omega_1-\omega-i\eta}{\Omega_{LO}}\right)^{-2} P^2q^2 \times \sum_{l=1}^{4}(P^2q^2)^{-1}\langle v|\vec{P}|c\rangle_l\langle c|\vec{P}|v\rangle_l \times\left[q^2-(\vec{e}_l\cdot\vec{q})^2\right]. \quad (16)$$

$\vec{P}$ is the momentum operator, P the magnitude of $\langle v|\vec{P}|c\rangle$ for $\vec{P}$ perpendicular to the corresponding Λ-direction. Thus, the sum is responsible for the selection rules whereas the dispersion is given by $[(\omega_1-\omega-i\eta)/\Omega_{LO}]^{-2}$. We write the tensor $\langle v|\vec{P}|c\rangle_l\langle c|\vec{P}|v\rangle_l$ as equal to $P^2\vec{\vec{T}}_l$, with the following tensors for $\vec{\vec{T}}_l$:

$l=1$: (111) $l=2$: $(1\bar{1}\bar{1})$

$$T_1=\frac{1}{6}\begin{bmatrix}2&-1&-1\\-1&2&-1\\-1&-1&2\end{bmatrix},\quad T_2=\frac{1}{6}\begin{bmatrix}2&1&1\\1&2&-1\\1&-1&2\end{bmatrix},$$

$l=3$: $(\bar{1}1\bar{1})$ $l=4$: $(\bar{1}\bar{1}1)$ (17)

$$T_3=\frac{1}{6}\begin{bmatrix}2&1&-1\\1&2&1\\-1&1&2\end{bmatrix},\quad T_4=\frac{1}{6}\begin{bmatrix}2&-1&1\\-1&2&1\\1&1&2\end{bmatrix}.$$

Near a two-dimensional critical point the electric susceptibility can be represented by a logarithmic singularity.[19] The most dispersive term of its second derivative with respect to the photon energy has the following form:

$$\frac{d^2\chi}{d\omega^2}=\frac{4\sqrt{3}}{9\pi}\frac{1}{a_0}\frac{1}{\omega}(\omega_1-\omega-i\eta)^{-2}. \quad (18)$$

If we substitute this into Eq. (16) and assume $3P^2/\omega_1\approx 1/m^*$ (see Ref. 21) we obtain a result for the Raman tensor similar to that near a three-dimensional critical point

$$\vec{\vec{R}}_F=\frac{3}{16}\frac{qC_F}{m^*}(S_e-S_h)\vec{\vec{F}}\frac{d^2\chi}{d\omega^2}, \quad (19)$$

with

$$\vec{\vec{F}}=\sum_l \vec{\vec{T}}_l[q^2-(\vec{e}_l\cdot\vec{q})^2]/q^2.$$

It is possible near E_1 to observe forbidden Raman scattering by LO phonons due to Fröhlich interaction not only in parallel but also in crossed configurations of incident and scattered light. However the strongest scattering is still expected in parallel-parallel configuration. For $q\parallel(110)$ we obtain for example for

$$e_i\parallel e_s=3^{-1/2}(1\bar{1}1):\quad F_{\parallel}=\tfrac{20}{27},$$

for

$$e_i=3^{-1/2}(111)\perp e_s=6^{-1/2}(1\bar{1}\bar{2}):\quad F_{\perp}=\tfrac{2}{27}\sqrt{2}\approx\tfrac{1}{7}F_{\parallel}.$$

We should point out that the result of Eq. (19) differs from that of Manuel *et al.*[22] who calculated the Raman tensor near a two-dimensional critical point (in their case a semiconductor superlattice) and found it to be proportional to $d\chi/d\omega$. The reason for this discrepancy is the fact that in the superlattice case the effect is not forbidden (i.e., $\propto q^2$), but allowed and induced by the difference in the electron and hole density for quantized states within a given superlattice slab.[23]

III. EXPERIMENTS

The experiments were performed in the usual backscattering configuration. Ar^+, Kr^+, He-Cd, and a jet-stream dye laser were used as exciting light sources. With the dyes rhodamine 6G, rhodamine B, cresyl violet, nile blue, and DMOTC, the red and near-infrared region, from 5700 to 8300 Å, were covered. The scattered light was analyzed either with a Jarrell Ash 1m or with a Spex 0.8-m double monochromator and detected with a RCA 31034 photomultiplier by photon counting.

As samples we used either (110) cleavage planes of undoped bulk material ($n\approx 10^{16}$ cm^{-3}) or (100) and (110) surfaces coated with high-quality layers, a few micrometers thick, grown by liquid phase epitaxy ($n<10^{15}$ cm^{-3}).

Unfortunately no dyes of high enough output power were available in the blue region below 4400 Å and in the infrared above 8500 Å. Thus we chose the possibility of tuning the gaps with respect to a fixed gas laser line. By varying the temperature between 80 and 700 K the E_1 gap was shifted according to Refs. 24 and 25 from 2.98 to 2.71 eV. Between 80 and 300 K the $E_0+\Delta_0$ gap was tuned from 1.85 to 1.77 eV.[26] The application of a hydrostatic pressure up to 70 kbar opened the E_0 gap from 1.43 to ~2.2 eV.[27] Thus, we were able to study the dispersion of the Raman cross section

near $E_1/E_1+\Delta_1$ and further below the E_0 gap.

Unless otherwise specified, all data shown will be corrected for the difference in temperature and pressure as referred to room temperature and zero pressure by shifting the photon energy according to the known temperature and pressure coefficients of the gaps. The data presented also contain corrections for the instruments response and the prefactors in Eqs. (1) and (2), the most important being ω^4 and the penetration depth of the light. For this purpose several absorption spectra were available originating from transmission measurements by Sturge[26] between 1.3 and 2.7 eV and by Cardona and Harbeke[24] between 1.6 and 3.2 eV, Kramers-Kronig transformed reflectivity data by Philipp and Ehrenreich[28] between 2.7 and 3.3 eV and ellipsometry data by Aspnes[29] above 2.5 eV. Aspnes and Philipp and Ehrenreich's data are believed to be the most accurate above 2.7 eV. Their difference is less than 20%. However the transmission data are by a factor of 2 smaller, probably because of pin holes in the very thin films which had to be used in these experiments. Thus, we took up to 2-eV Sturge's data, adjusted in the transparent region by our own measurements. Above 2.7 eV the data of Philipp and Ehrenreich were used, and in the region from 2 to 2.7 eV we interpolated between both sets of data. The resulting error in the absorption correction performed in this manner is believed to be smaller than 50%, which gives an error in the deduced Raman tensor of less than 20%.

IV. RESULTS AND DISCUSSION

Figure 1 shows the Γ_1 and Γ_{15} components of the second-order Raman spectrum taken at a photon energy of 2.81 eV. The corresponding Γ_{12} component is negligible. Similar to the other zinc-blende materials investigated so far, the Γ_1 spectrum of GaAs is composed mainly of overtones of phonons with high density of states. The assignments were made by comparison with neutron scattering data.[30] Between 100 and 230 cm^{-1} scattering by 2TA phonons is observed, around 450 cm^{-1} scattering by 2LA and between 490 and 550 cm^{-1} scattering by TO overtones. In addition, a structure due to TO+ TA scattering is observed between 300 and 400 cm^{-1}. As first-order scattering is allowed only in Γ_{15} symmetry the peaks at the TO and LO(Γ) frequencies are due to slight misorientation of the light inside the sample plus a contribution from forbidden LO scattering.

In the case of second-order deformation potential scattering by overtones, the Γ_1 spectrum should reflect the weighted density of phonon states with the energy scale multiplied by 2. The

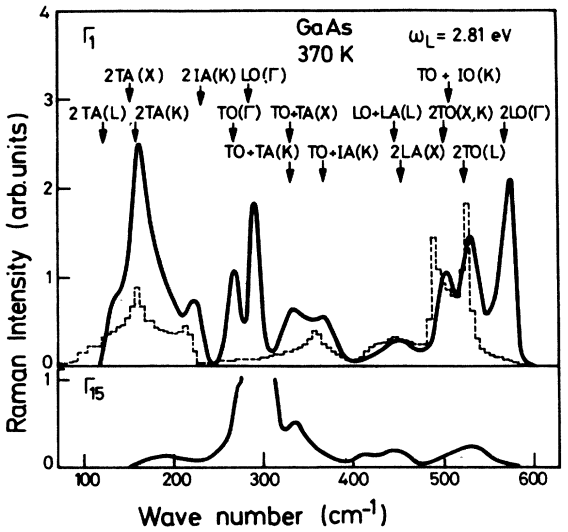

FIG. 1. Γ_1 and Γ_{15} components of the Raman spectrum of GaAs.

dashed line represents a density of states calculation by Go[31] based on the bond charge model. It is in basically good agreement with the experimental spectrum except for the peak at the 2LO(Γ) frequency which, as we shall see later, is due to a different coupling mechanism.

For the Γ_{15} spectrum an identification of the observed structure is not so definite. The peak at 330 cm^{-1} is clearly due to TO-TA scattering. We label the structures between 400 and 460 cm^{-1} as LA+ LO and that between 490 and 550 cm^{-1} as TO + IO(LO), where IO is an optical phonon with q ∥ (110) and neither transverse nor longitudinal polarization.

In Fig. 2 the resonance behavior of first-order scattering by TO phonons near the E_1 critical points is shown. The fact that a broad maximum is observed more or less between E_1 and $E_1+\Delta_1$ indicates that the three-band term dominates in Eq. (10). Thus, the fits shown are made with the expression $|(\chi^+-\chi^-)/\Delta_1|^2$. Two methods were used to extract χ^+ and χ^- from the experimental data which we took from Aspnes[29]:

(i) Sell and Kane[32] made for Ge the assumption that both contributions χ^+ and χ^- are of the same shape and magnitude, only shifted in energy by Δ_1. The separation can then be made iteratively for the imaginary parts of the susceptibility while the real parts can be obtained from the Kramers-Kronig relations. We found however that the result for $\chi^+-\chi^-$ can be also extracted directly from the experimental data. The curve calculated this way for GaAs was not completely satisfactory (see Ref. 33). After introducing the possibility of χ^+ and

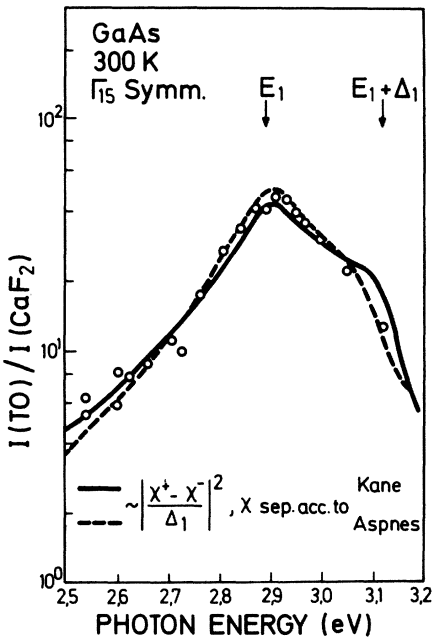

FIG. 2. E_1 resonance of first-order Raman scattering by TO phonons in Γ_{15} symmetry.

χ^- being of unequal magnitude, the excellent fit shown was obtained for $\chi^-(\omega+\Delta_1)=0.8\chi^+(\omega)$.

(ii) The second curve shown in Fig. 2 was calculated from data received by a similar separation process proposed by Aspnes.[34] Best results were achieved in this case for $\chi^-(\omega+\Delta_1)=0.5\chi^+(\omega)$. Thus, both fits indicate that indeed the E_1 contribution to the electric susceptibility is stronger than that of the $E_1+\Delta_1$ transition. There are three possible reasons for this inequality: (a) Due to the $\vec{k}\cdot\vec{p}$ coupling between the spin-orbit-split valence bands, the transverse effective mass of the upper valence band is larger than that of the lower one.[35] (b) The susceptibility is proportional to ω^{-2} (see Ref. 21) which also makes χ^- smaller than χ^+. (c) Possible Lorentz field corrections[36] may make χ^+ larger than χ^-.[36]

The curves shown are shifted slightly in energy in order to obtain the best agreement with the experimental results. In Table I the shifts between all theoretical and experimental resonance curves near E_1 for first- and second-order scattering are summarized. The reason why these values deviate from the expected $+\frac{1}{2}\Omega$ or $+\frac{1}{2}(\Omega_1+\Omega_2)$ has not yet been clarified. However, also in other crystals investigated so far, the values obtained for E_1 by resonant Raman experiments deviate slightly from the ones obtained by other measurements.[10,12] The fact that different shifts were necessary in GaAs for the curves as calculated by the two separation procedures indicates that these shifts need not be of fundamental character.

TABLE I. Energy shifts of theoretical curves near E_1 to give best fit with the experimental points which are plotted as a function of the laser energy (in meV).

TO(Γ)	Separation according to Kane	+15±5
	Separation according to Aspnes	−35±5
Forbidden. LO		+15±5
2LO(Γ)	in Γ_1 symmetry	−30±5
2TA	in Γ_1 symmetry	−25±5
2TO	in Γ_1 symmetry	−30±5
TO+TA	in Γ_1 symmetry	−20±5
TO+TA	in Γ_{15} symmetry	−100±10
TO+IO	in Γ_{15} symmetry	−100±10
LA+LO	in Γ_{15} symmetry	−75±10

Near the three-dimensional critical points all shifts observed were, within the experimental error, the ones expected, that means the resonance maxima occured at an energy $\frac{1}{2}\Omega$ or $\frac{1}{2}(\Omega_1+\Omega_2)$ higher than the gap energies. Scattering by LO phonons was measured in allowed crossed configuration near $E_1/E_1+\Delta_1$ and around $E_0+\Delta_0$ and showed the same resonance behavior as the TO phonons. Due to the electro-optical effect, however, the scattering intensity for LO phonons was found to be about 30% stronger than that by TO phonons.[6]

In Fig. 3 we show the dispersion of the Raman

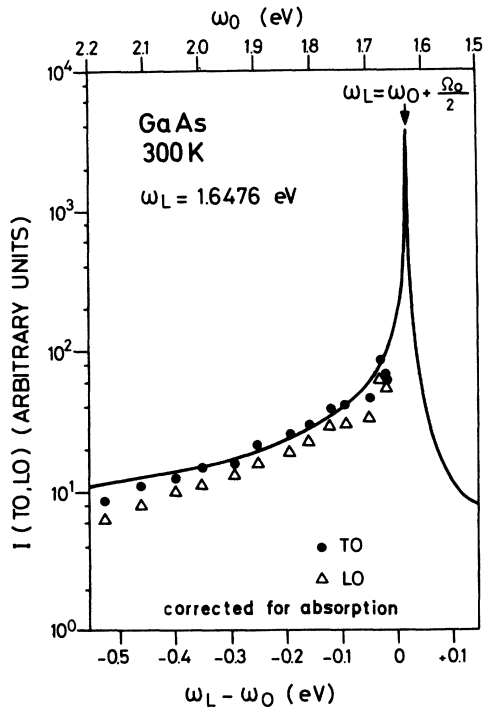

FIG. 3. Pressure induced E_0 resonance of the Raman phonons of GaAs.

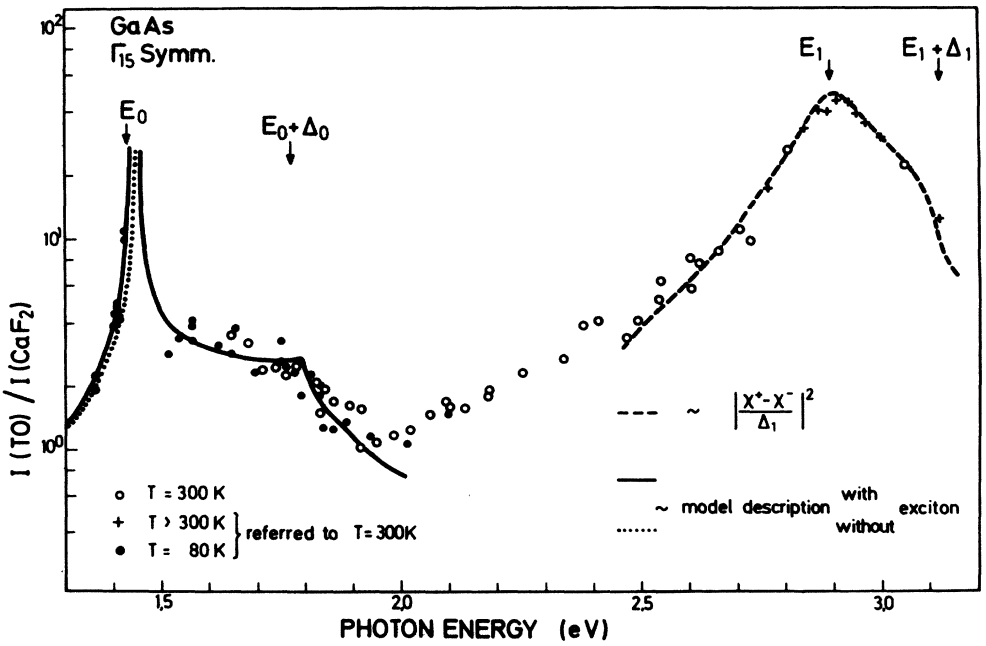

FIG. 4. Resonance behavior of Raman scattering by TO phonons near the $E_0/E_0+\Delta_0$ and the $E_1/E_1+\Delta_1$ energy gaps.

cross section for first-order scattering below the fundamental (E_0) gap. These measurements were performed by pressure tuning of the gaps. No attention should be paid to the relative strength of TO and Lo because the orientation of the light inside the pressure cell was not known. The fit shown was made with the model description for χ of Eq. (8). In order to refer the strength of this resonance to that at $E_1/E_1+\Delta_1$ we shall need the constant prefactor of Eq. (8). It was adjusted in order to give the best fit to the imaginary part χ_2 in the photon energy region from 1.52 to 2.0 eV.

Figure 4 shows the dispersion of the scattering intensity by TO phonons in the entire region between 1.35 and 3.1 eV. We have included in this figure the line shape of the E_0 resonance obtained with and without exciton contributions. The steep increase below the fundamental gap is better fitted by taking the exciton contribution to χ into account.

As we now have a good theoretical description of the Raman cross section near $E_0/E_0+\Delta_0$ and near the $E_1/E_1+\Delta_1$ gaps, we can determine from Eq. (3) and (10) the ratio of the electron–one-phonon deformation potential near $E_1(d^5_{3,0})$ to that near $E_0(d_0)$. The result obtained is $d^5_{3,0}/d_0 = 0.6 \pm 50\%$. In contrast to this a pseudopotential calculation based on the rigid-ion model yields 1.3 for this ratio.[37] This is just outside our quoted error in which estimate the experimental error, a possible error in the χ values used in Eqs. (3) and (10) and the possible error in the absorption correction are included. We believe that effects of the small penetration depth of the light inside the crystal in the blue spectral region, e.g., exciton free surface layers, should be included automatically in the experimental χ values we used. Due to convergence problems of the used pseudopotential wave functions near E_1 and to inaccuracies in the rigid-ion model the calculation may give a too high value for $d^5_{3,0}$. This idea is supported by a calculation of $d^5_{3,0}$ for silicon done by Goroff and Kleinman[38] with orthogonalized-plane-wave wave functions. They obtained a value which is more than a factor of 2 smaller than that obtained by Zeyher for Si.[2] In contrast, the results obtained by both authors for d_0 are about the same.

Raman scattering by LO phonons was studied in forbidden configuration with $q \| (110)$ near $E_0+\Delta_0$ and near E_1. In Fig. 5 we present data taken at 80 K near the $E_0+\Delta_0$ transition. The vertical scale is in units of the TO scattering intensity at the energy of the $E_0+\Delta_0$ gap. The solid line was obtained from Eq. (14) with a broadening $\eta = 0.3\Omega_{LO}$. Measurements taken at liquid-helium temperature showed exactly the same resonance behavior. The resonance at room temperature required a fit with a broadening of $\eta = 0.45\Omega_{LO}$. The dashed line in Fig. 5 was obtained with Eq. (15) by using the experimental χ values from Refs. 26 and 39. Instead of the second derivative we used the first derivative to the third power which should be a better description of the data. Both fitting curves represent the experimental variation of the Raman

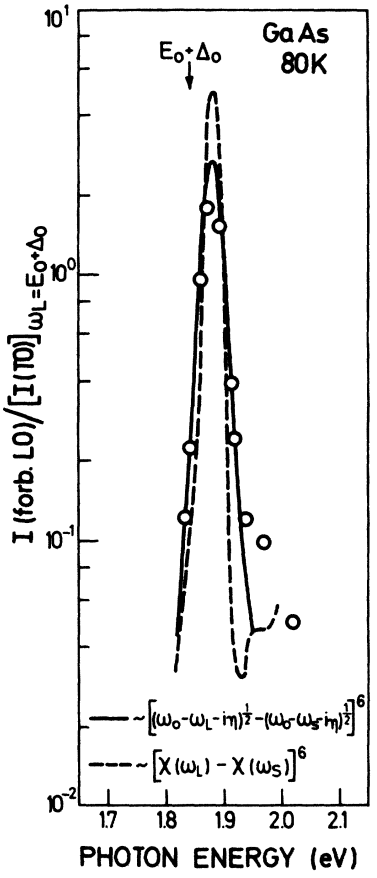

FIG. 5. Resonance of forbidden Raman scattering by LO phonons at the $E_0+\Delta_0$ gap. The intensity scale is in units of the TO scattering cross section taken with $\omega=1.975$ eV.

cross section rather well. Thus a quantitative comparison of the observed forbidden LO intensity with that of the allowed TO scattering should be made. From Eqs. (3) and (15) we obtained with

TABLE II. Parameters used to calculate intensities of forbidden LO scattering at $E_0+\Delta_0$ and at E_1.

	$E_0+\Delta_0$		E_1
m_e	0.066[a]		0.063[b]
m_h	0.16[a]		...
s_e-s_h	...		$\frac{1}{3}$[c]
a_0 (Å)		5.6537[d]	
ϵ_∞		11.10[e]	
ϵ_0		13.13[e]	
$d_0, d_{3,0}^5$ (eV)	31.5[f]		41[f]
ω_L (eV)	1.875		2.81
T (K)	80		370

[a] Reference 45. [c] Reference 21. [e] Reference 48.
[b] Reference 46. [d] Reference 47. [f] Reference 37.

the parameters given in Table II for a photon energy of 1.875 eV and 80 K $I(\text{forb LO})/I(\text{TO}) = 1.7 \pm 1.0$. This is in excellent agreement with the experimentally observed value of 1.6. Thus the Fröhlich coupling mechanism explains not only qualitatively but also quantitatively the forbidden LO scattering near $E_0+\Delta_0$ and that suggested by Gogolin and Rashba[8] does not seem to be operative here. In Fig. 6 data taken near the E_1 transition are shown for two samples of different carrier concentration. The vertical scale is in units of the TO scattering intensity at the energy of the E_1 gap. We first discuss the "undoped" sample ($n=1.8\times10^{16}$ cm^{-3}). Here a good agreement be-

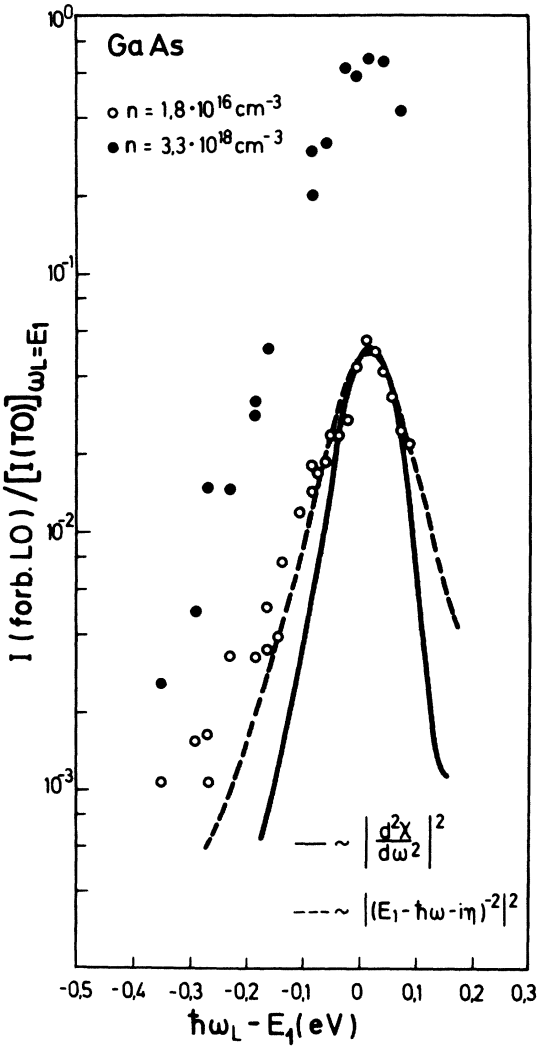

FIG. 6. Resonance of forbidden Raman scattering by LO phonons near the E_1 gap. The intensity scale is in units of the TO scattering cross section taken with $\omega=2.9$ eV.

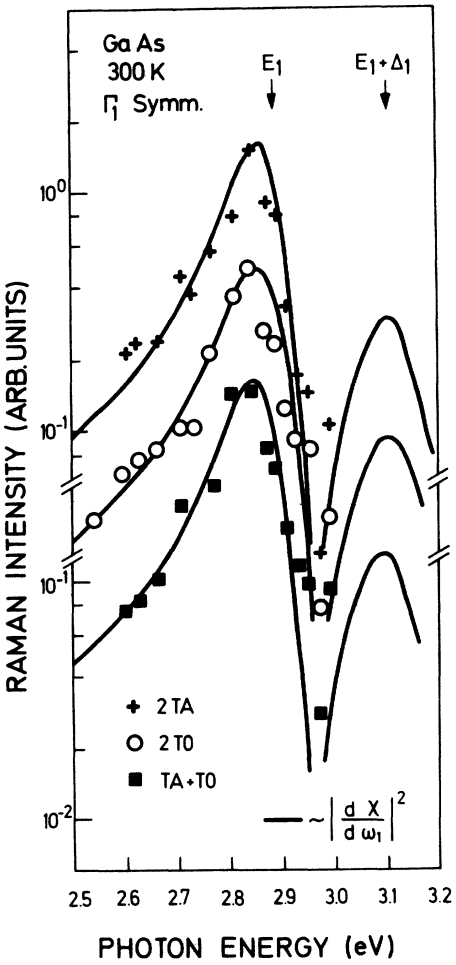

FIG. 7. E_1 resonance of several second-order Raman processes in Γ_1 symmetry.

tween experiment and the theory of Eq. (18) can be obtained only for a broadening as high as $\eta = 3\Omega_{LO}$ (dashed line). Using the experimental values, in Eq. (19) the agreement is not satisfactory (solid line). One should however note that the peak intensity is much lower relative to that of the TO scattering than for the $E_0+\Delta_0$ resonance. Thus, slight misorientation of the light inside the sample or other mechanisms which make a fraction of allowed LO scattering observable would alter the shape of the measured resonance curve more than near $E_0+\Delta_0$. In order to make a quantitative comparison we therefore took data for $\omega - E_1 = 0.05$ eV, close to the resonance maximum, where such effect would be smaller. From Eqs. (10) and (19) follows with the parameters of Table II that $I(\text{forb LO})/I(\text{TO}) = 0.25 \pm 0.15\%$, which is again in good agreement with the experimental value of 0.19. Thus, as in the case of the $E_0+\Delta_0$ gap, we can explain forbidden LO scattering near $E_1/E_1+\Delta_1$ by means of the q-dependent Fröhlich coupling.

As a possibility for an additional contribution we discuss the effect of a surface electric field. According to a result given by Zeyher[40] the Raman tensor is in this case proportional to the electric field and the third derivative of the electric susceptibility with respect to the photon energy. For our undoped sample we obtain with a Schottky barrier model the surface electric field to be of the order of 10^4 V/cm. This value would give a Raman intensity comparable with the one obtained for Fröhlich coupling. Thus we studied a "doped" crystal with $n = 3.3 \times 10^{18}$ cm^{-1} for which the electric field is of the order of 10^5 V/cm. From theory we thus expect an increase in the Raman intensity of a factor of 100, much larger than the experimental increase which is just one order of magnitude. A possible explanation may be a partial shorting out of the field by photocarriers. In any case, a more thorough investigation of the electric field induced forbidden LO scattering would be desirable.

In order to obtain information about the electron-two-phonon coupling the resonance behavior of the second-order structures was investigated. Figure 7 shows the variation of the Raman cross section near E_1 for three of the peaks observed in Γ_1 symmetry. A description by Eq. (11) fits the experimental data very well so that an interpretation in terms of the renormalized electron-two-phonon deformation potential interaction is valid. That is the case also for the structures observed in Γ_{15} symmetry (Fig. 8). However, in Γ_{15} symmetry intra- as well as interband scattering is allowed. Because of the existence of two independent three- and two-band deformation potentials, their ratio was adjusted in order to obtain a good fit to the experimental data. For all three peaks shown a best fit was found for $D_1^5/D_3^5 \approx 0.4$. Clearly the three-band term dominates. From the ratio of second- to first order scattering intensities we could evaluate not only the deformation potential of Γ_1 symmetry D_1 but also the three-band deformation potential of Γ_{15} symmetry D_3^5. We summarize the results in Table III.[41] The 2 LA scattering intensity was measured only at one photon energy.

In contrast to the structures discussed so far the 2LO(Γ) peak observed in Γ_1 symmetry showed a much stronger dispersion near E_1 (Fig. 9). Only an iterated electron–one-phonon scattering process explains this behavior. In this case, perturbation theory gives us three resonating denominators in the Raman tensor instead of two for the renormalized electron–two-phonon process.[18]

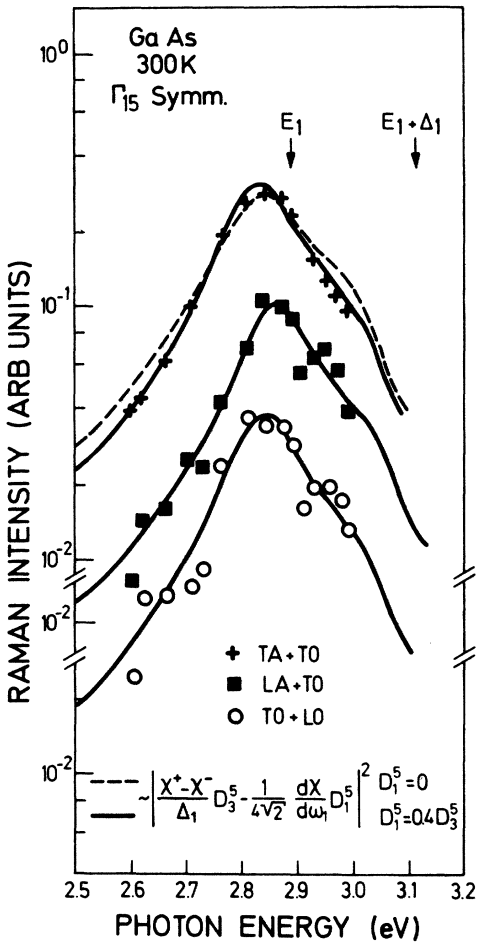

FIG. 8. E_1 resonance of several second-order Raman processes in Γ_{15} symmetry.

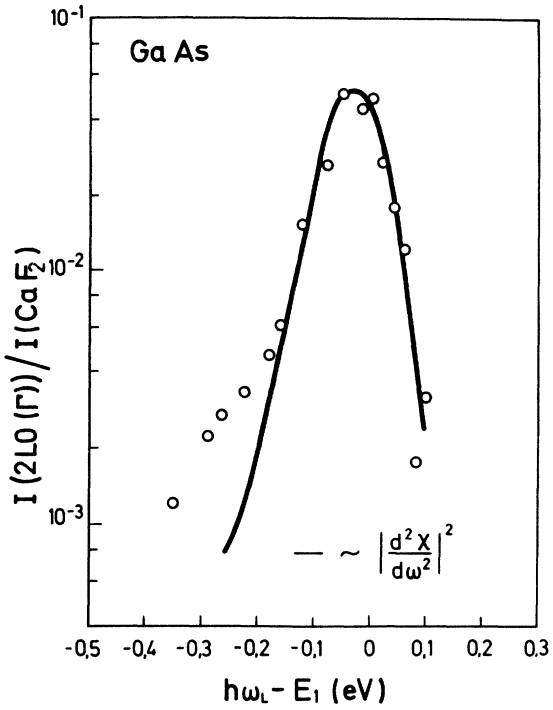

FIG. 9. E_1 resonance of the 2LO(Γ) peak in Γ_1 symmetry.

Due to the vanishing density of states of the scattering phonons such a contribution is small far away from resonance. Since we do not observe a similar 2TO(Γ) scattering as well we conclude that the electron–one-LO-phonon coupling re-

TABLE III. Electron–two-phonon deformation potentials for the isoelectronic crystals Ge, GaAs, and ZnSe (in eV).

		D_1	D_3^5/D_{15}	D_3^3
GaAs (E_1)	2TA	450		
	TO+TA	550	140	
	2LA	670		
	2TO	2070		
	LO+LA		390	
	TO+IO		470	
GaAs (E_0)	2TO	2600		
Ge (E_1)	2TA	170		
	2TO	2534	543	470
ZnSe (E_0)	2TA	545		
	TO+TA		250	
	TO+LO		260	
	2LO	510		

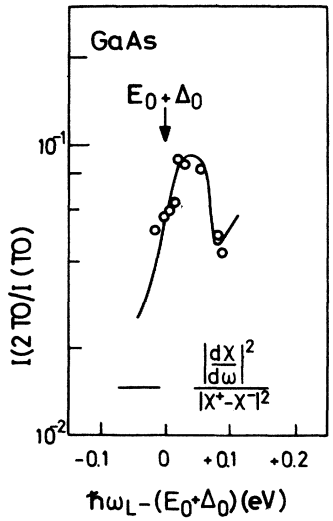

FIG. 10. $E_0+\Delta_0$ resonance of 2TO scattering in Γ_1 symmetry with respect to TO scattering.

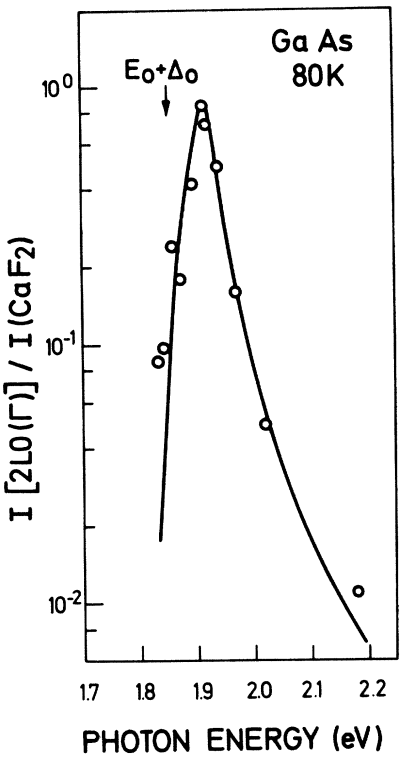

FIG. 11. $E_0+\Delta_0$ resonance of the 2LO(Γ) peak in Γ_1 symmetry. The solid line represents the theory of Ref. 44.

quired for the 2LO(Γ) resonance is the Fröhlich interaction. The experimental data are fitted well by $|d^2\chi/d\omega^2|^2$.

Near $E_0+\Delta_0$ we were able to measure only the resonance behavior of the optical overtones in Γ_1 symmetry. Figure 10 shows the ratio of 2TO to 1TO scattering intensities as a function of photon energy relative to the gap. A maximum close to $E_0+\Delta_0$ is observed in contrast to the first-order Raman effect. The curve shown is calculated with Eq. (4) using the experimental values and with Eq. (3) using the model description. In view of the good agreement between theory and experiment we can obtain the electron–two-TO-phonon deformation potential D_1 for $E_0+\Delta_0$ which should be the same as for E_0 (the spin-orbit splitting is not likely to be affected by the phonon). Its value is given also in Table III. For a comparison we display the deformation potentials derived by Renucci *et al.*[10] for the E_1 gap in Ge and by Schmidt[5] for the E_0 gap in ZnSe. It should be noted that the electron–two-phonon deformation potentials near E_1 are evaluated for both Ge and GaAs with respect to the electron–one-phonon deformation potential $d^5_{3,0}(E_1)$ as calculated with pseudopotential wave functions. They should be scaled down if this value turns out to be smaller, as suggested here. If we now compare the electron–two-phonon deformation potentials in the isoelectronic series Ge-GaAs-ZnSe two trends can be seen: Coupling of electrons to two TA phonons decreases with decreasing covalent bonding whereas coupling to two optical phonons increases. We can only make the following attempt at an interpretation of this fact. According to the model of ionic polarizabilities developed by Kunc and Bilz[42] for ionic crystals the increasing cation to anion mass ratio is responsible for the increasing coupling of electrons to two optical phonons measured by Schmidt and Cardona[43] in the series ZnTe-ZnSe-ZnS. This would be in agreement with the trend for the isoelectronic crystals. Decreasing 2TA scattering would thereafter be attributed to a stronger polarizability of the Se with respect to the As and to Ge.

The 2LO(Γ) scattering shows a very sharp resonance behavior near $E_0+\Delta_0$ (Fig. 11) as in the case of the E_1 gap. Again we explain this by means of an iterated electron–one-LO-phonon scattering due to the Fröhlich coupling. Numerical calculations of the Raman cross section were done for this scattering process by Abdumalikov and Klochikhin.[44] The solid line in Fig. 11 represents their calculation for an electron to hole mass ratio 0.19 and a damping $\eta=0.4\Omega_{LO}$. It is in very good agreement with our experimental results.

V. CONCLUSIONS

GaAs is an excellent material for resonant Raman studies since two sets of gaps ($E_0/E_0+\Delta_0$, $E_1/E_1+\Delta_1$) fall within a region in which continuous lasers and a number of discrete laser lines exist. We have identified the mechanisms for allowed scattering by one phonon (two-band processes at E_0, three-band processes at $E_0+\Delta_0$, E_1, and $E_1+\Delta_1$) and by two phonons (two-band processes for Γ_1 scattering at $E_0/E_0+\Delta_0$, $E_1/E_1+\Delta_1$, mainly three-band processes for Γ_{15} scattering at $E_1/E_1+\Delta_1$). The scattering by 2LO(Γ) phonons is a fourth-order process produced by the Fröhlich interaction.

We have also investigated the forbidden LO(Γ) resonances near $E_0+\Delta_0$ and E_1. The shape of these resonances agrees with the predictions of the forbidden (q-dependent) Fröhlich mechanism. Its strength can also be quantitatively accounted for on this basis.

By assuming for the optical-phonon deformation potential of the Γ_{15} valence bands the calculated value ($d_0=31.5$ eV) we have been able to determine

from the fits to the resonance curve the one-phonon deformation potentials at $E_1/E_1+\Delta_1$ and a number of electron–two-phonon deformation potentials at both sets of gaps. The latter fit well into the systematics of similar deformation potentials obtained before for other members of the germanium–zinc-blende family.

ACKNOWLEDGMENTS

We would like to thank Dr. E. Anastassakis, Dr. A. Pinczuk, and Dr. R. Zeyher for many helpful discussions, Dr. E. Bauser for preparing the epitaxial grown surfaces, and Dr. W. Holzapfel for his help with the pressure experiments.

[1]F. Cerdeira, W. Dreybrodt, and M. Cardona, Solid State Commun. 10, 591 (1972).
[2]J. B. Renucci, R. N. Tyte, and M. Cardona, Phys. Rev. B 11, 3885 (1975).
[3]B. A. Weinstein and M. Cardona, Phys. Rev. B 8, 2795 (1973).
[4]R. L. Schmidt, B. D. McCombe, and M. Cardona, Phys. Rev. B 11, 746 (1975).
[5]R. L. Schmidt, Ph.D. thesis (Stuttgart, 1976) (unpublished).
[6]W. D. Johnston, Jr. and I. P. Kaminow, Phys. Rev. 188, 1209 (1969).
[7]M. I. Bell, in *Proceedings of the International Conference on the Physics of Semiconductors* (PWN-Polish Scientific, Warzaw, 1972), p. 845.
[8]A. A. Gogolin and A. E. Rashba, in *Proceedings of the 13th International Conference on the Physics of Semiconductors*, edited by F. G. Fumi (Tipografia Marves, Rome, 1976), p. 284.
[9]B. A. Weinstein and M. Cardona, Phys. Rev. B 7, 2545 (1972).
[10]M. A. Renucci, J. B. Renucci, R. Zeyher, and M. Cardona, Phys. Rev. B 10, 4309 (1974).
[11]B. A. Weinstein and M. Cardona, Solid State Commun. 10, 961 (1972).
[12]W. Kiefer, W. Richter, and M. Cardona, Phys. Rev. B 12, 2346 (1975).
[13]R. Trommer and M. Cardona, Solid State Commun. 21, 153 (1977).
[14]R. Loudon, J. Phys. 26, 677 (1965).
[15]M. Cardona, Solid State Commun. 9, 819 (1971).
[16]R. Zeyher, T. S. Ting, and J. L. Birman, Phys. Rev. B 10, 1725 (1974).
[17]R. M. Martin, Phys. Rev. B 4, 3676 (1971).
[18]B. A. Weinstein, thesis (Brown University, 1974) (unpublished).
[19]A. S. Davydov, *Quantum Mechanics* (Pergamon, Oxford, 1965).
[20]E. O. Kane, Phys. Rev. 178, 1368 (1969).
[21]M. Cardona, in *Atomic Structure and Properties of Solids* (Academic, New York, 1969).
[22]P. Manuel, G. A. Sai-Halasz, L. L. Chang, Chin-An Chang, and L. Esaki, Phys. Rev. Lett. 37, 1701 (1976).
[23]A. Pinczuk (private communication).
[24]M. Cardona and G. Harbeke, J. Appl. Phys. 34, 813 (1962).
[25]F. Lukes and E. Schmidt, in *Proceedings of the International Conference on the Physics of Semiconductors*, Exeter (Institute of Physics and Physical Society, London, 1962), p. 389.
[26]M. D. Sturge, Phys. Rev. 127, 768 (1962).
[27]B. Welber, M. Cardona, C. K. Kim, and S. Rodriguez, Phys. Rev. B 12, 5729 (1975).
[28]H. R. Philipp and H. Ehrenreich, in *Semiconductors and Semimetals*, edited by R. K. Willardson and A. C. Beer (Academic, New York, 1967), Vol. 3, Chaps. 4 and 12.
[29]D. E. Aspnes (private communication).
[30]J. L. T. Waugh and G. Dolling, Phys. Rev. 132, 2410 (1963).
[31]S. Go (private communication).
[32]D. D. Sell and E. O. Kane, Phys. Rev. 185, 1103 (1969).
[33]R. Trommer, E. Anastassakis, and M. Cardona, in *Light Scattering in Solids*, edited by M. Balkanski, R. C. C. Leite, and S. P. S. Porto (Flammarion, Paris, 1976), p. 396.
[34]D. E. Aspnes (unpublished).
[35]M. Cardona, Phys. Rev. B 15, 5999 (1977).
[36]J. A. van Vechten and R. M. Martin, Phys. Rev. Lett. 28, 446 (1972).
[37]R. Zeyher (private communication).
[38]I. Goroff and L. Kleinman, Phys. Rev. 132, 1080 (1963).
[39]D. D. Sell and S. E. Stokowski, in Proceedings of the Tenth International Conference on the Physics of Semiconductors, Cambridge, Mass. (USAEC, Oak Ridge, Tenn., 1970).
[40]R. Zeyher and W. Richter (unpublished).
[41]Due to a calculation error the numbers for the deformation potentials D_1 given in Ref. 29 are by a factor of 2 too large.
[42]K. Kunc and H. Bilz, Solid State Commun. 19, 1027 (1976).
[43]R. L. Schmidt and M. Cardona, in Ref. 7, p. 239.
[44]A. A. Abdumalikov and A. A. Klochikhin, Phys. Status Solidi B 80, 43 (1977).
[45]K. Hess, D. Bimberg, N. O. Lipari, J. U. Fischbach, and M. Altarelli, in Ref. 8, p. 142.
[46]D. E. Aspnes (private communication).
[47]R. W. G. Wyckoff, *Crystal Structures* (Wiley, New York, 1965), Vol. I.
[48]S. Iwasa, I. Balslev, E. Burstein, in *Proceedings of the Seventh International Conference on the Physics of Semiconductors*, edited by M. Hulin (Dunod, Paris, 1964), p. 1077.